Research Article
Vol. 31, No. 2 / 16 Jan 2023 / *Optics Express* 826
Optics EXPRESS

Predicting strongly localized resonant modes of light in disordered arrays of dielectric scatterers: a machine learning approach

Mohammad Ali,[1,3] A. K. M. Naziul Haque,[1,2,3] Nafis Sadik,[1] Tashfiq Ahmed,[1] and Md Zunaid Baten[1,*]

[1] *Department of Electrical and Electronic Engineering, Bangladesh University of Engineering and Technology, Dhaka, Bangladesh*
[2] *Department of Computer Science and Engineering, Brac University, Dhaka, Bangladesh*
[3] *These authors contributed equally to this work*
[*] *mdzunaid@eee.buet.ac.bd*

Abstract: In this work, we predict the most strongly confined resonant mode of light in strongly disordered systems of dielectric scatterers employing the data-driven approach of machine learning. For training, validation, and test purposes of the proposed regression architecture-based deep neural network (DNN), a dataset containing resonant characteristics of light in 8,400 random arrays of dielectric scatterers is generated employing finite difference time domain (FDTD) analysis technique. To enhance the convergence and accuracy of the overall model, an auto-encoder is utilized as the weight initializer of the regression model, which contains three convolutional layers and three fully connected layers. Given the refractive index profile of the disordered system, the trained model can instantaneously predict the Anderson localized resonant wavelength of light with a minimum error of 0.0037%. A correlation coefficient of 0.95 or higher is obtained between the FDTD simulation results and DNN predictions. Such a high level of accuracy is maintained in inhomogeneous disordered media containing Gaussian distribution of diameter of the scattering particles. Moreover, the prediction scheme is found to be robust against any combination of diameters and fill factors of the disordered medium. The proposed model thereby leverages the benefits of machine learning for predicting the complex behavior of light in strongly disordered systems.

1. Introduction

Disordered photonics – an area of photonic research that is governed by random scattering mediated interference of light in disordered media –has become an exciting area of research over the recent years [1,2]. Among different exotic phenomena of light in disordered systems, Anderson localization or the strong localization of light is one of the most intriguing ones not only because of the rich physics associated with it [3], but also because of its potential applications in the areas of lasing [4,5], energy harvesting [6], sensing [7] and imaging [8]. The wavelength and Q-factor of strongly localized modes in a disordered system are strongly dependent on the spatial profile of dielectric constant of the medium, and they tend to change drastically with its spatial profile. Consequently, the localization characteristics of light in disordered media cannot be predicted analytically, and must instead be obtained through rigorous experiments [9–11] or numerical techniques like finite difference time domain simulation [12–14]. An entirely different approach is to employ a data-driven technique like machine learning, in which a self-sufficient mathematical model can be trained such that it can predict attributes related to the complex behavior of light in a disordered medium.

Over the past several years, there has been a growing interest in the area of data-driven research in photonics, in which different machine learning techniques have been successfully employed to

#475495 https://doi.org/10.1364/OE.475495
Journal © 2023 Received 13 Sep 2022; revised 25 Nov 2022; accepted 27 Nov 2022; published 3 Jan 2023

model and design photonic structures [15–17]. In particular, deep neural networks (DNN) have been found to be very effective to model the complex non-linear relationships between inputs and outputs of photonic systems. Different multi-layered models of DNNs have been successfully employed to solve inverse problems related to photonics, in which photonic structures are designed based on the desired optical response [18–21]. DNNs have found their way in the solution of forward problems as well, where the electromagnetic responses are predicted for a well-defined photonic structure [22–25]. Such forward and inverse problem related applications of DNNs have been primarily aimed towards the design and analysis of ordered photonic structures involving metamaterials and metasurfaces [18,26–29], plasmonic systems [20,30–32] and photonic crystals [25,33,34]. More recently there have been efforts toward leveraging the potential of DNNs for the analysis of disordered photonic structures. The impact of introducing disorder in two-dimensional (2D) photonic crystal nanocavities have been reported in [23,25], where the cavity quality factor has been predicted with a high degree of accuracy using DNNs. In another work, the localized mode area of 2D structures produced by random displacement of an original square lattice has been predicted based on convolutional and fully-connected layers of DNNs [35]. Several deep learning-based studies involving random speckle patterns have also been reported in the context of imaging of random scattering media [36,37]. In spite of these significant advances in machine learning-enabled photonics, the prospect of utilizing such techniques for predicting the behavior of light in strongly-disordered media has remained unexplored. In particular, it remains to be seen if machine learning techniques can be reliably applied to predict the Anderson localized resonant modes of light in practical strongly disordered systems.

In the present study, we investigate the prospect of predicting the strongly localized resonant modes of light in a uniform random array of dielectric scatterers representing self-organized GaN nanowire arrays grown by molecular-beam epitaxy. Based on experimentally reported dimensionalities of such systems, 8400 samples of representative disordered arrays have been systematically generated and considered in this work. The strongly localized resonant modes of these random arrays have been estimated by electromagnetic simulations employing finite difference time domain analysis technique. The problem of identifying the most strongly confined resonant modes in these arrays is subsequently categorized as a machine learning problem, where an auto-encoder network is utilized to create a lower-dimensional encoded representation of the original input vector. From the prediction of the convolutional neural network (CNN) – which consists of three convolution layers followed by three fully connected layers – the figure of merits has been estimated and compared with the simulation results. The results of our model suggest that the proposed machine learning approach can capture the interlink between the random positions of the dielectric scatterers and the strong-localization characteristics of light with a high degree of accuracy. The model thereby offers a novel means of predicting the Anderson localized resonant modes of light in strongly disordered media of dielectric scatterers.

2. Methods and analyzed structures

The disordered media considered in this study represent GaN-based self-organized nanowire arrays grown by molecular beam epitaxy (MBE). This material system has been extensively studied for the experimental realization of optoelectronic devices and systems involving lasers, LEDs, photodiodes, optical waveguides, and photonic integrated circuits [9,10,38,39]. The Anderson localization phenomenon of light has also been extensively studied and reported based on such systems both from theoretical and experimental standpoints [11–13,40]. In what follows, we discuss the methodology employed to generate the spatial profiles of the disordered systems considered in this work. Also, the finite difference time domain (FDTD) simulation technique applied to create the reference dataset is discussed herein.

2.1. Generation of random nanowire arrays

In accordance with previous reports on Anderson localization of light in self-organized GaN nanowire arrays grown on (001) Si substrate, $3\mu m \times 3\mu m$ arrays of nanowires have been considered in this work. The considered size of the array ensures that the disordered medium is significantly larger than the localization area necessary to observe the strong localization of light. An isometric view of the sample nanowire array and its corresponding two-dimensional cross-section are shown in Figs. 1. For the considered GaN-based system, strong localization of light ranging from UV-A to UV-C regime has been reported for nanowire diameters ranging from 50-80 nm. Furthermore, it has been reported that in order to attain random-scattering mediated strong-localization of light, a minimum fill-factor of 30% is essential in GaN-based systems [41]. Based on these observations, different combinations of diameters and fill-factors of the nanowires have been considered to systematically generate uniform random arrays of dielectric scatterers.

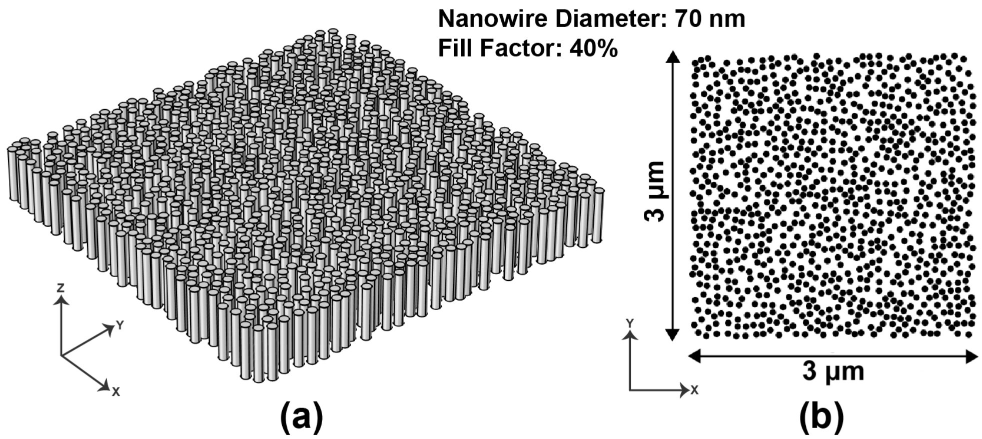

Fig. 1. (a) Three-dimensional (3D) schematic of the isometric view of a representative nanowire array and (b) its corresponding two-dimensional (2D) cross-section.

A detailed description of different configurations of the nanowire arrays considered in this work is graphically shown in Fig. 2. For each fill-factor ranging between 30-55%, two different distributions of the nanowire diameters are considered. In the first case, each array is considered to be a homogeneous scattering medium having a constant diameter (d) of the nanowires. In the second and more realistic case of a disordered medium having scatterers of different dimensions, a Gaussian distribution profile of nanowire diameters is considered. In this case, a standard deviation (σ) of nanowire diameter is maintained in each array such that 3σ equals 10% of the mean diameter ($\bar{d}$) of the nanowires. Based on this approach, seven different constant (mean) diameters ranging from 50 nm to 80 nm have been considered to generate the homogeneous (inhomogeneous) disordered arrays in this work. For each set of diameter and fill-factor, 100 spatial configurations of the nanowires have been considered. This ultimately results in a total of 8400 random arrays of dielectric scatterers. From this sample space, 6048, 1520, and 832 arrays have been exclusively considered for training, validation, and test purposes, respectively.

2.2. FDTD analysis of generated arrays

The strong-localization characteristics of light in the 8400 sample arrays considered in this work have been evaluated based on finite difference time domain (FDTD) analysis technique, employing open source software package MEEP [42]. In doing so, two-dimensional (2D) cross-sections of the sample arrays (similar to the case of Fig. 1(b)) have been considered. It is to be noted that FDTD simulations results obtained from the analysis of 2D cross-sections of self-organized

Optics EXPRESS

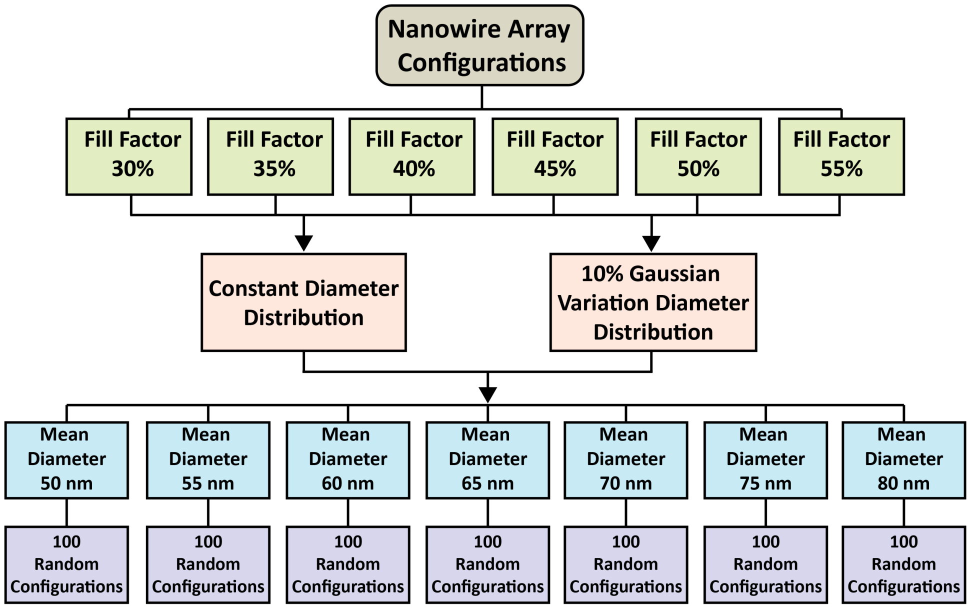

Fig. 2. A graphical summary of different configurations of the 8,400 nanowire arrays generated in this work based on reported diameters and fill-factors of epitaxially grown self-organized nanowire arrays.

nanowire arrays are found to be consistent not only with 3D simulations results [40], but also with experimental observations [11,39]. This is owing to the fact that strong localization of light in practical nanowire arrays is governed by the in-plane random scattering phenomena. Consequently, even though in practice the self-organized nanowires are usually 1-2 μm long, strong-localization characteristics can be reasonably predicted considering infinite length of these nanowires. Hence in our FDTD simulation, we have considered infinite length of the nanowires along the z-direction to reduce computational cost and also to eliminate length-dependence of the simulation results. Considering the wavelength of interest, the GaN permittivity is taken to be 6.76 in accordance with experimental results. This corresponds to a refractive index value of 2.6.

In accordance with previous theoretical studies on strong localization of light in a disordered medium, optical loss i.e. material absorption has not been considered in our FDTD simulations. It is understandable that in real systems there will be light absorption at photon energies above the optical bandgap. In spite of such absorption, the multiple-scattering mediated localization of light will prevail in the randomly distributed nanowires. As has been demonstrated by experiments [11,14], in the case of direct bandgap materials like GaN or InP, the random nanowires will not only constitute among themselves a mirrorless cavity but will also form the gain medium to demonstrate lasing behavior around the resonance wavelength. As the present study aims to offer a generalized framework to predict the random scattering mediated resonance of light in disordered arrays of any dielectric scatterers, the optical loss has not been considered herein. It is also known that nitride-based disordered systems are better suited for the strong localization of transverse magnetic (TM) mode of light [12]. Hence, the present study considers a TM-polarized Gaussian pulse source at the center of each array to obtain the strong-localization characteristics of light in the corresponding disordered medium. A perfectly matched layer having a thickness greater than the source wavelength has been considered throughout the study to ensure that any non-resonant mode leaking out from the array does not reflect back. The resonant modes and localization strengths – quantified in terms of quality factor (Q-factor) – have been obtained by

Optics EXPRESS

decomposition of the field components of the optical wave using filter diagonalization method [43]. Resonant characteristics obtained from FDTD simulations of two representative disordered arrays having nanowire diameters of 50 nm and 80 nm, and a fill-factor of 40% are shown in Fig. 3. As can be observed from Figs. 3(b) and 3(c), the most strongly confined modes of these arrays have Q-factors in the order of 10^5. The electric field distributions of these modes (shown in Figs. 3(a) and 3(c)) exhibit the signature of strong localization of light. It is noteworthy that for the array having d = 50 nm, the resonant wavelength of the mode having the highest Q-factor is centered around 227 nm, whereas for the d = 80 nm array, the most strongly confined mode is located around 400 nm. This is consistent with previous reports on Anderson localization of light in nitride systems, where the localization wavelength is observed to vary from UV-C to near-visible wavelength regime depending on scatterer diameter [11,12]. The dependence of resonant wavelength on nanowire diameter is shown in greater detail in Fig. 4 which plots as a function of nanowire diameter the resonant wavelength of the most strongly confined mode of each of the 8400 arrays. As can be observed, for each diameter, the resonant wavelength varies by approximately ±50 nm around the center wavelength. Such a high degree of variability is attributed to the randomness associated with the spatial configurations of the arrays. The variation of fill-factor over a wide range of 30% to 55% also contributes to the variability of resonant wavelength for fixed diameters of the arrays. In spite of such variability, a systematic red-shift of resonant wavelength occurs as the mean diameter increases from 50 nm to 80 nm. It is also noteworthy that this characteristic dependence of localization wavelength on nanowire diameter is obtained with an equal number of random arrays for each set of diameter and fill factor of the nanowires. This effectively forms a balanced dataset, which is essential for an unbiased prediction using machine learning [44].

It is to be noted that in previous studies, it has been observed that extended but high Q-factor whispering gallery-type resonant modes are attained in weakly disordered rotationally symmetric systems because of internal reflections from the sample boundaries [41]. However, for the disordered systems under consideration, it is observed that in general, the highest Q-factor mode tends to have the strongest spatial localization of the optical field. In Fig. 5, we show near field images of the localized modes of a representative array, where the Q-factors vary from 10^6 to 10^2. As can be observed, for high-Q resonant modes, electric fields are confined/localized in a tight space, whereas for low-Q modes, electric fields are extended over a larger area, and tend to leak away from the system in a much shorter time. This demonstrates a one-to-one correspondence between localization and Q-factor of the self-organized nanowire-like disordered systems under consideration.

Optics EXPRESS

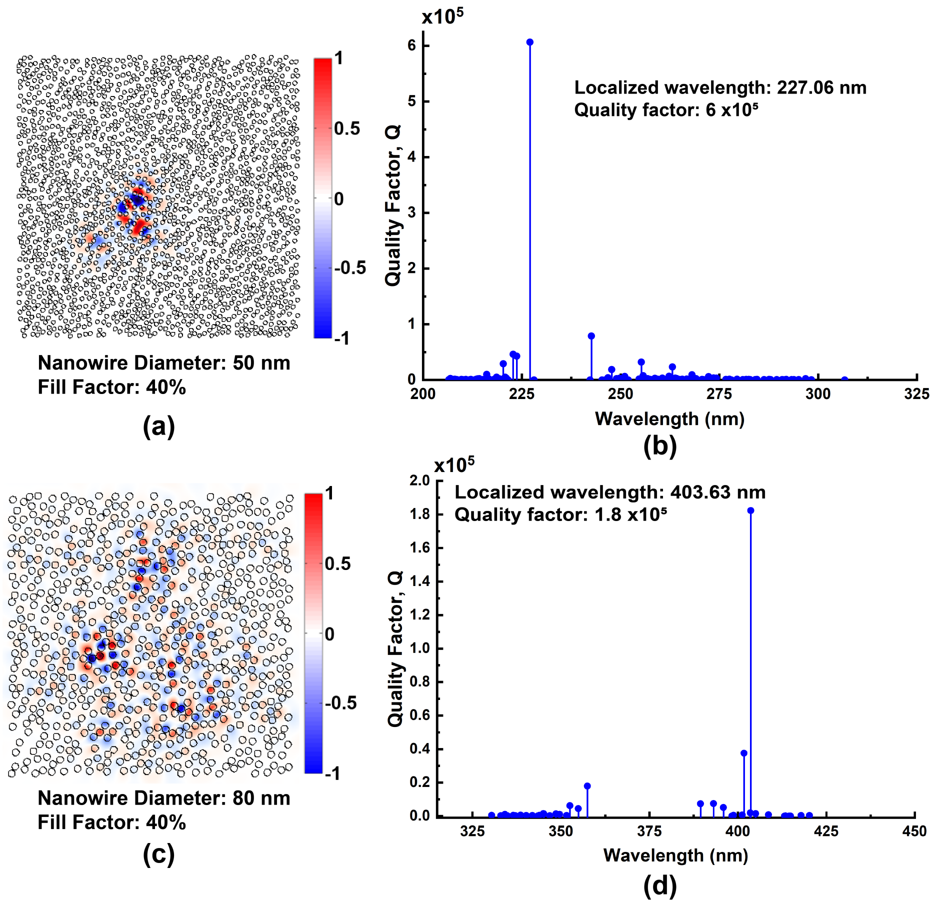

Fig. 3. Finite difference time domain (FDTD) simulation results of the (a) electric field distribution of the resonant mode of a single random realization of nanowire array having d = 50 nm and fill-factor 40%, and (b) the corresponding quality factor plotted as a function of wavelength. (c) FDTD simulation results of electric field distribution of the resonant mode of a single random realization of nanowire array having d = 80 nm and fill-factor 40% and (d) the corresponding quality factor plotted as a function of wavelength

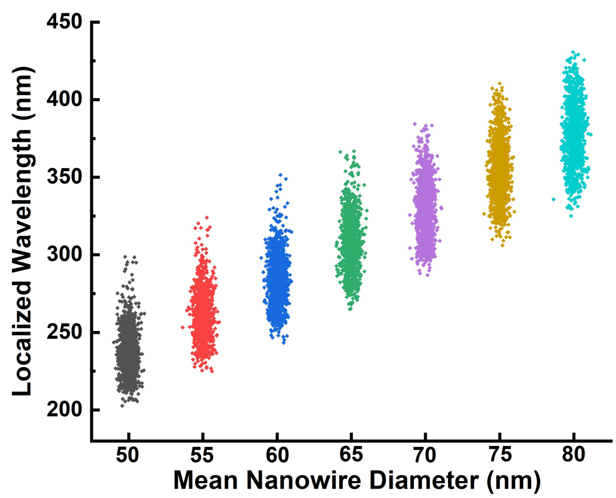

Fig. 4. Scatter plot of the finite difference time domain (FDTD) analysis based simulation results of the most strongly confined resonant mode of light in the 8,400 uniform random arrays having mean diameters ranging from 50 nm to 80 nm.

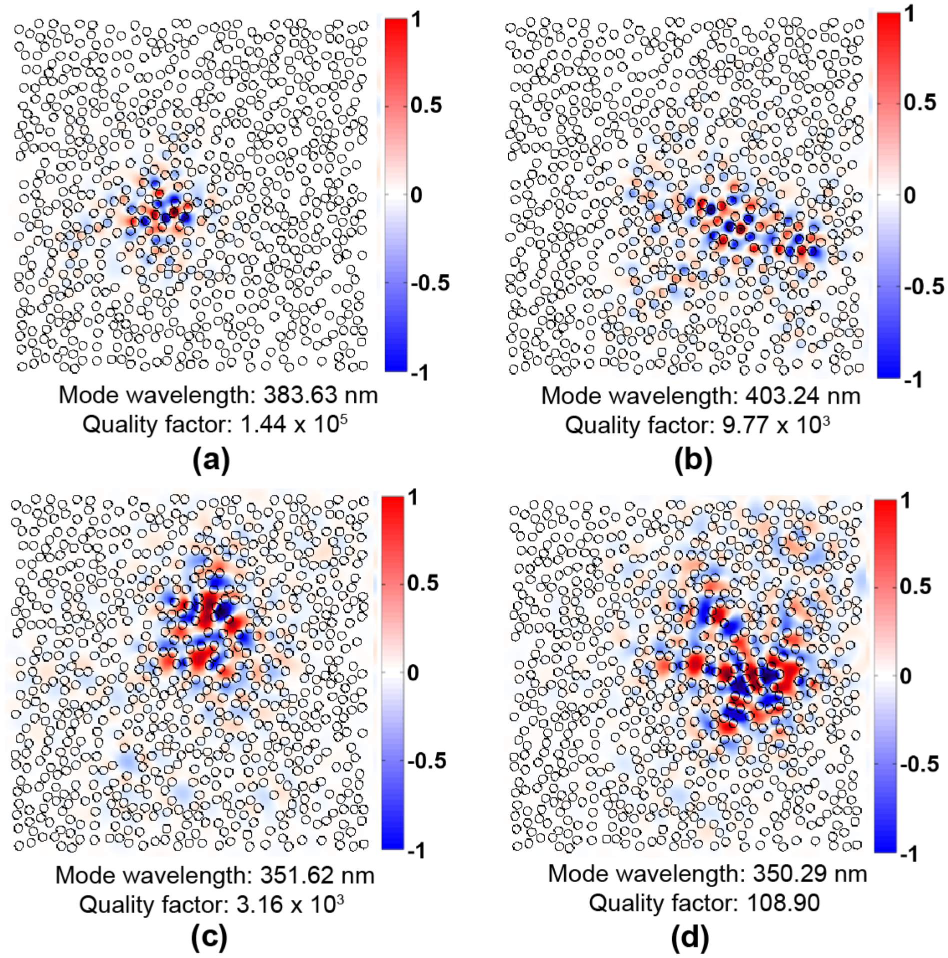

Fig. 5. Electric field distribution of the resonant modes for a single configuration having (a) quality factor of 1.44×10^5 and localized wavelength of 383.63 nm, (b) quality factor of 9.77×10^3 and localized wavelength of 403.24 nm. (c) quality factor of 3.16×10^3 and localized wavelength of 351.62 nm. (d) quality factor of 108.90 and localized wavelength of 350.29 nm.

3. Deep learning model architecture

The deep learning-based model architecture proposed in this work consists of a regression model, together with an autoencoder-based learning scheme. The autoencoder is employed for weight initialization of the regression model, which is subsequently utilized for predicting the most strongly localized resonant mode of a disordered array. In our proposed scheme, refractive index profiles of the random arrays are used as inputs to the deep neural network. A preprocessing step is performed prior to applying the array as an input to the DNN. In this step, the refractive index profile of an array is mapped into a 374×374 pixel gray-scale image and min-max normalization is performed to ensure that all elements of the image lie within zero and one. In what follows, we discuss the proposed deep neural network-based model in detail.

3.1. Autoencoder model architecture

An autoencoder neural network – which is commonly utilized for medical image analysis [45,46] – is an unsupervised learning algorithm that conducts backpropagation by setting the target values to be equal to the inputs [47]. This algorithm is particularly useful for weight initialization of deep neural networks for prediction purpose [48–50]. It promotes faster convergence of the regression model and minimizes the likelihood that the solution will converge on a local minima. As shown in Fig. 6(a), the autoencoder model utilized in this work is divided into encoder and decoder blocks. The encoder compresses the input gray-scale image of an array and produces an encoded version of the image. The encoder block consists of multiple convolution layers and each convolution block is followed by a maxpooling block to gradually reduce the resolution of the input image.

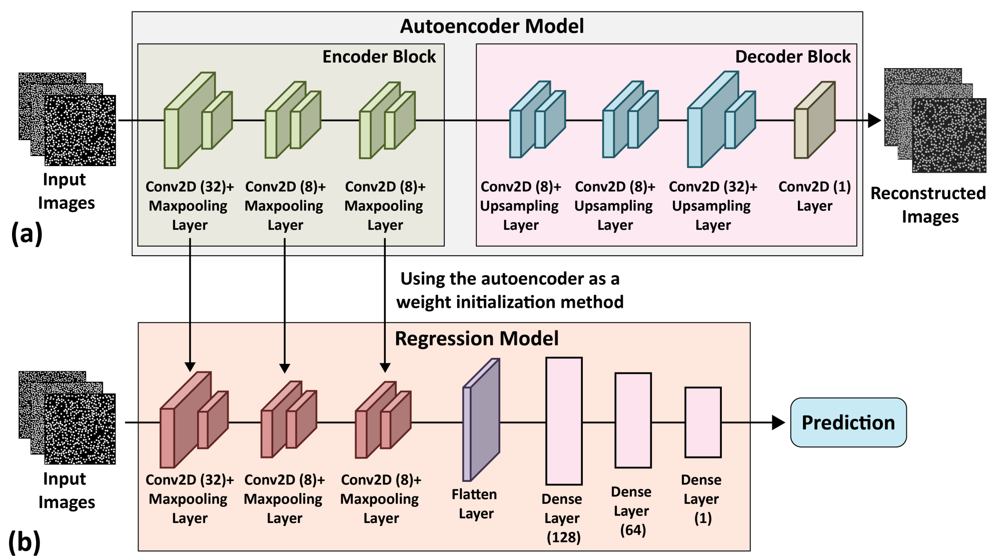

Fig. 6. Schematic illustration of the proposed deep learning architecture showing different layers of the (a) autoencoder model comprising of encoder and decoder blocks, and (b) the regression model that predicts localization wavelength of the disordered medium based on the image given as its input.

In this study, a total of three convolution (Conv2D) layers and three maxpooling layers have been used to construct the encoder. The encoder converts the input images of size (374, 374, 1) into encoded data of size (47, 47, 8). The decoder block, likewise consists of three convolution layers. However, in this case, each convolution layer is followed by an upsampling layer which steadily increases the resolution of the encoded data. Therefore the decoder block is essentially a mirror opposite of the encoder which recovers the original images from the encoded version of the image. At the end of the decoder block, there is a convolution layer that has the same number of channels as the input image. This convolution layer utilizes a linear activation function, whereas all the previously described layers contain Relu activation function. During the compression and reconstruction process of the encoder and decoder block, the autoencoder model learns and preserves the unique properties of the images of the dataset. These features are eventually employed for prediction purposes when the fine-tuned weights of the encoder are utilized for initializing the regression model.

3.2. Regression model architecture

The regression model architecture proposed in this work takes as input 374×374 pixel gray-scale images generated from the refractive index profiles of the disordered arrays. In order to exploit the fine-tuned weights of the encoder from the previous step, the initial convolution and maxpooling layers used in the regression model are kept identical to those of the encoder block of the autoencoder model architecture. Hence the output of the third maxpooling layer of the regression model is a dataset of size (47, 47, 8). The output of this layer is passed through a flatten layer, which converts the multi-dimensional array of pooled feature map into a single long continuous linear vector. The flattened output is a feature vector of length 17672, which is provided as input to two fully connected dense layers, with the first one having 128 neurons and the second one having 64 neurons. Finally, the output of the second dense layer is passed through a fully connected dense layer containing a single neuron with linear activation. This layer gives as output wavelength of the most strongly localized resonant mode of the disordered array under consideration. A schematic illustration of the regression model architecture is shown in Fig. 6(b).

3.3. Training and validation scheme

The proposed autoencoder and regression model architectures were implemented with the Keras library utilizing Tensorflow 2.0 backend. In the first stage of training, the autoencoder was randomly initialized and optimized based on the Adam optimization technique [51]. The mean square error (MSE), which is defined by the following loss function, is minimized during this optimization step.

$$MSE = \frac{1}{N}\sum_{i=1}^{N}(x_i - y_i)^2$$

Here N is the number of data points, x_i is the observed value, and y_i is the predicted value. Based on the 6048 random arrays segregated for training, the autoencoder was trained for 200 epochs with a batch size of 32. The weights of the layers of the encoder block were next utilized to initialize the weights of the first six layers of the regression model architecture. The model was found to converge relatively fast, within 25 epochs. An adaptive learning rate is utilized to allow the training algorithm to monitor the performance of the model, and to automatically modify the learning rate for optimal performance. To this end, the 1520 random arrays isolated for validation purposes were utilized. In our adaptive learning scheme, if the validation loss does not improve for 3 successive epochs, the learning rate is gradually reduced in steps from 10^{-3} to 10^{-5} with a factor of 0.1. Also to minimize overfitting, early interruption of the training process has been incorporated in case the validation loss does not improve for 8 consecutive epochs.

4. Results and discussion

In order to assess the performance characteristics of the proposed autoencoder model architecture, its learning curve, which is essentially the MSE loss between the original and reconstructed images, is plotted as a function of the number of epochs in Fig. 7(a). As can be observed, the loss falls rapidly within the first few epochs and then decreases monotonically. Original images of representative nanowire arrays and their corresponding reconstructed images obtained from the autoencoder model are shown in Fig. 7(c). The high quality of the reconstructed images confirms good convergence of the autoencoder model architecture. As the regression model architecture utilizes the autoencoder as a weight initializer for its convolution and maxpooling layers, it achieves convergence within a few epochs. This is further illustrated in Fig. 7(b), which shows the training and validation losses of the regression model. Even though the training loss initially remains high, it decreases within the first few epochs and then almost gets saturated. The validation loss follows a similar trend, thereby confirming the fast convergence of the regression model. The prediction losses obtained for the regression model are in accordance with MSE values obtained for reported regression architecture-based prediction techniques [52,53].

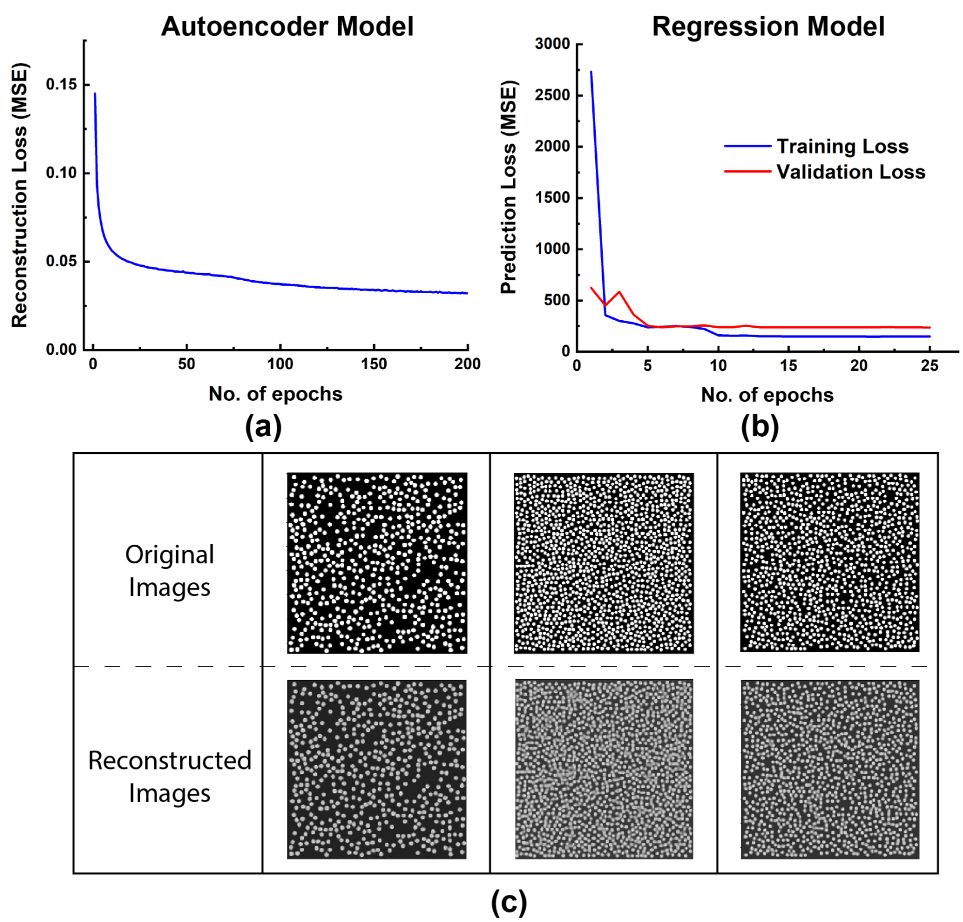

Fig. 7. (a) Learning curve of the autoencoder model showing the reconstruction loss in terms of mean square error (MSE), plotted against the number of epochs. (b) Prediction loss, defined in terms of MSE, during training and validation steps of the regression model plotted as a function of the number of epochs. (c) Original images of the random arrays, along with their reconstructed counterparts obtained as the output of the autoencoder model described in Fig. 5(a).

Optics EXPRESS

To quantify the prediction performance of the proposed model, the Pearson correlation coefficient (R) is utilized which is defined as follows.

$$R = \frac{\sum_{i=1}^{n}(\lambda_{FDTD\,i} - \overline{\lambda_{FDTD}})(\lambda_{NN\,i} - \overline{\lambda_{NN}})}{\sqrt{\sum_{i=1}^{n}(\lambda_{FDTD\,i} - \overline{\lambda_{FDTD}})^2}\sqrt{\sum_{i=1}^{n}(\lambda_{NN\,i} - \overline{\lambda_{NN}})^2}}$$

Here λ_{FDTD} is the target resonant wavelength obtained from FDTD simulations, λ_{NN} is the resonant wavelength obtained by the proposed DNN model, n is the number of test samples, and $\overline{\lambda_{FDTD}}$ and $\overline{\lambda_{NN}}$ are mean values of the target wavelengths obtained by FDTD and DNN techniques respectively. The correlation between λ_{FDTD} and λ_{NN} is graphically shown for training and test datasets in Figs. 8(a) and 8(b) respectively. For both cases, the results appear around the unity-slope line, which suggests a strong correlation between predicted and actual values. For the training dataset, the correlation coefficient between λ_{FDTD} and λ_{NN} is obtained to be 0.9695, and for the test dataset, the value is 0.9546. Similar order of correlation coefficients has been reported in other DNN-enabled prediction schemes applied to photonic research [24,25].

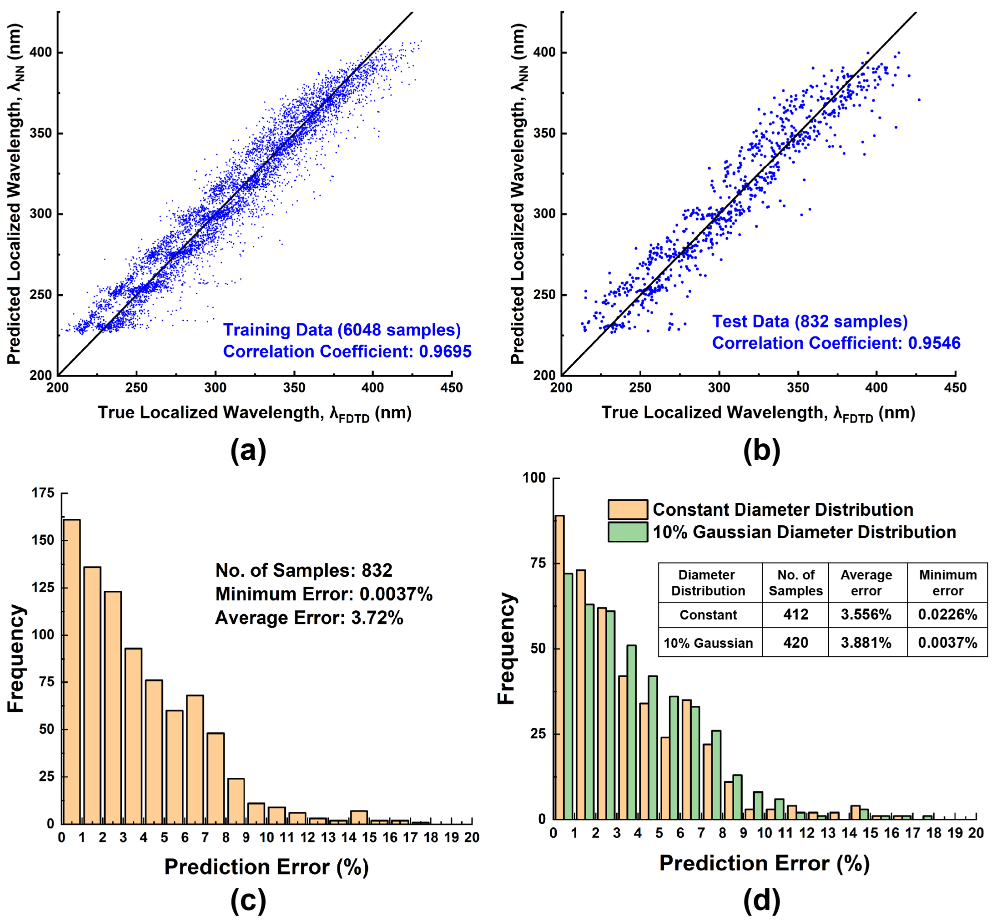

Fig. 8. Performance evaluation of the proposed deep learning model architecture plotted in terms of actual localization wavelength (λ_{FDTD}) and deep learning model predicted localization wavelength (λ_{NN}) obtained for the (a) training and (b) test dataset. (c) Distribution of prediction errors for the 832 test dataset. (d) Comparison of prediction errors for constant and Gaussian diameter cases of 412 and 420 random arrays respectively.

Optics EXPRESS

It is noteworthy that in the test dataset, 412 out of the total 832 samples contained nanowire arrays of constant diameters, whereas the remaining 420 samples contained arrays having a Gaussian distribution of the diameter – defined as per the random array generation scheme described in Section 2.1. The correlation coefficient between predicted and actual localization wavelengths for the arrays of constant diameter is obtained to be $R = 0.9583$. This value is slightly higher than the correlation coefficient, $R = 0.9515$ obtained for the Gaussian distributed case. To further evaluate the performance characteristics of the prediction scheme, a second figure of merit ϵ_{abs} is defined on the basis of the absolute difference between the predicted and actual value of localization wavelength.

$$\epsilon_{abs} = \frac{|\lambda_{NN} - \lambda_{FDTD}|}{\lambda_{FDTD}} \times 100\%$$

The resultant histogram plot obtained for ϵ_{abs} values of the test dataset is shown Fig. 8(c). For the test set of 832 samples, the average value of ϵ_{abs} is 3.72%, with the minimum error being 0.0037%. The histogram plot shows that for the majority of the samples, the prediction error ϵ_{abs} is less than 5%. Considering the fact that the study is based on strongly disordered random arrays, the accuracy obtained with the DNN model is substantial for a reasonable prediction of localized wavelengths of self-organized GaN nanowire arrays. To compare the case of the constant diameter arrays with the case of arrays having Gaussian distributed diameters, prediction errors (ϵ_{abs}) obtained for the test dataset are shown in the histogram plot of Fig. 8(d). The average error for the constant diameter case is 3.556% and for the inhomogeneous diameter case, the value is 3.881%. Therefore, the prediction errors and the Pearson correlation coefficients confirm that the model makes a better prediction if the disordered system contains scatterers of identical diameters. Nonetheless, as the accuracy levels for the inhomogeneous and homogeneous diameter cases are very close, it can be suggested that the model is robust enough to predict localization wavelengths of practical systems with a reasonably high degree of accuracy.

Finally, to understand whether the proposed model is biased towards nanowire arrays of particular diameters or areal densities, the prediction errors are plotted as a function of mean diameters and fill factors of the nanowire arrays of the test dataset. The results, shown in Fig. 9, indicate that the prediction errors for all diameters and fill-factors vary within a common range. Moreover, the mean prediction errors for arrays of different diameters and fill-factors are also fairly similar. To be precise, the mean prediction error for different diameters varies from 3.329% to 5.178%, whereas for different fill-factors the mean prediction error varies from 3.334% to 4.21%. These results confirm that the proposed architecture – instead of being biased towards any particular areal density or diameter – performs equally well for any combination of diameter and fill factor of the nanowires. The box-and-whisker plot of Fig. 9 also depicts the first quartile (Q1), median (Q2), third quartile (Q3), and the interquartile range (IQR) of prediction errors for different nanowire diameters and fill-factors of the arrays. It is observed that for only a few cases the prediction error lies above the top whiskers. The presence of such a few numbers of outliers is indicative of the robustness of the machine learning model. In terms of time and computational burden, it is observed that with identical computational resources, the fine-tuned deep learning model can predict localization wavelength at least 100-200 times faster than the time taken by the FDTD solver. This offers the prospect of utilizing the proposed machine learning model for the design and analysis of strongly disordered medium-based photonic and optoelectronic devices and systems. For cases where a very high degree of accuracy is required, the proposed deep learning approach can be used as a preliminary step to FDTD simulations, so that the range of inspection wavelength can be narrowed down quickly.

Optics EXPRESS

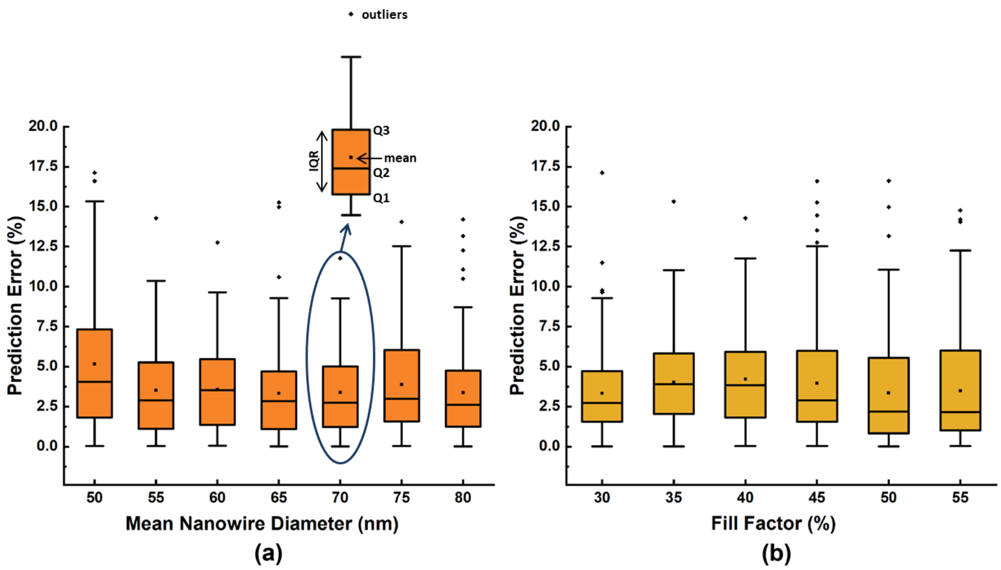

Fig. 9. Box plots showing prediction errors for training dataset having different (a) mean diameters and (b) fill factors of the nanowire arrays.

5. Extension of the proposed model

As has been discussed in Section 2, the proposed model is based on FDTD simulation results of 2D cross-sections of 3D nanowires, and these results are applicable for 3D arrays of scatterers where localization is governed by in-plane random scattering of light. This model can be further generalized to analyze fully random 1D and 3D systems as well. Localization of light has been experimentally demonstrated and theoretically studied in 1D systems like random stack of dielectrics [54] or irregular Bragg gratings [55]. By estimating localization characteristics of light in such systems using electromagnetic simulations, the ML model can be trained to predict high Q resonant modes of 1D systems. As far as 3D systems are concerned, strong localization of light has been found to be rather difficult to attain in 3D random structures because of the high refractive index contrast required in such systems. Recently there have been theoretical propositions regarding strong localization of light using 3D disordered systems of atoms [56] and amorphous dielectric networks [57]. Prediction of localization characteristics of light in such systems would necessitate the generation of a training dataset based on appropriate theoretical formalism and electromagnetic simulations. As the degrees of freedom are higher in 3D simulations, such studies are expected to be computationally expensive for a data-driven approach like machine learning.

As has been shown earlier in Fig. 5, a one-to-one correspondence exists between spatial localization and Q-factor of light in the disordered systems under consideration. The present study aimed to predict the localization wavelength of the most tightly confined mode, which in the present case is the highest Q-factor mode, and hence the machine learning model has been trained accordingly. The applicability of this model can be extended to predict the localization length of light in disordered systems as well. For this, a training dataset containing information on the spatial distribution of the optical field of the strongly confined modes has to be formed, and the ML model has to be trained based on this dataset. The model can also be extended to predict the highest Q factor mode of the cases where there are no localized modes - such as the cases of TM modes in a periodic structure or TE modes in a disordered one. For such cases, the machine learning model has to be trained with corresponding datasets, which should contain systematically

Optics EXPRESS

generated periodic/disordered arrays and corresponding electromagnetic simulation results. Furthermore, by considering optical absorption and material gain, the results and the machine learning model presented here can be extended to predict the lasing characteristics of random lasers.

6. Conclusion

In summary, a convolutional neural network-based regression model architecture has been proposed in this work to predict the strongly confined resonant mode of light in disordered media representing practical systems of dielectric scatterers. Based on experimentally reported attributes of epitaxially grown self-organized GaN nanowire arrays, 8,4000 random arrays have been generated and analyzed in this work to create the dataset necessary for training, validation, and testing of the machine learning model. The model can predict the wavelength of the most strongly localized mode of light – namely, the Anderson localized resonant mode – with a minimum error of 0.0037%. The correlation coefficients between the machine learning-based predictions and FDTD simulation results are higher than 0.95 for different diameters and areal densities of the dielectric scatterers. The forward model is observed to have no bias towards any diameter or areal densities of the arrays, and therefore it can predict the high-Q resonant mode of light for any combination of diameter and areal densities of the nanowires. Though the present work emphasized the prediction of Anderson localized resonant mode of light, the approach adopted here can be extended for accurate and fast solving of other disordered photonics-related forward problems, such as predicting quality factors, far-field directionality characteristics, the extent of spatial localization, and the number of resonant modes of light in strongly disordered systems.

Acknowledgments. The authors acknowledge the support and facilities obtained from the Department of Electrical and Electronic Engineering (EEE), Bangladesh University of Engineering and Technology (BUET). M.Z.B. acknowledges the support of the Basic Research Grant (reference no. r-60/re-4747) from Bangladesh University of Engineering and Technology.

Disclosures. The authors declare no conflicts of interest related to this article.

Data availability. Data underlying the results presented in this paper are not publicly available at this time but may be obtained from the authors upon reasonable request.

References

1. D. S. Wiersma, "Disordered photonics," Nat. Photonics **7**(3), 188–196 (2013).
2. S. Yu, C.-W. Qiu, Y. Chong, S. Torquato, and N. Park, "Engineered disorder in photonics," Nat. Rev. Mater. **6**(3), 226–243 (2021).
3. M. Segev, Y. Silberberg, and D. N. Christodoulides, "Anderson localization of light," Nat. Photonics **7**(3), 197–204 (2013).
4. D. S. Wiersma, "The physics and applications of random lasers," Nat. Phys. **4**(5), 359–367 (2008).
5. J. Liu, P. D. Garcia, S. Ek, N. Gregersen, T. Suhr, M. Schubert, J. Mørk, S. Stobbe, and P. Lodahl, "Random nanolasing in the Anderson localized regime," Nat. Nanotechnol. **9**(4), 285–289 (2014).
6. K. Vynck, M. Burresi, F. Riboli, and D. S. Wiersma, "Photon management in two-dimensional disordered media," Nat. Mater. **11**(12), 1017–1022 (2012).
7. S. H. Choi and Y. L. Kim, "The potential of naturally occurring lasing for biological and chemical sensors," Biomed. Eng. Lett. **4**(3), 201–212 (2014).
8. A. P. Mosk, A. Lagendijk, G. Lerosey, and M. Fink, "Controlling waves in space and time for imaging and focusing in complex media," Nat. Photonics **6**(5), 283–292 (2012).
9. T. Frost, S. Jahangir, E. Stark, S. Deshpande, A. Hazari, C. Zhao, B. S. Ooi, and P. Bhattacharya, "Monolithic electrically injected nanowire array edge-emitting laser on (001) silicon," Nano Lett. **14**(8), 4535–4541 (2014).
10. T. Frost, A. Hazari, A. Aiello, M. Z. Baten, L. Yan, J. Mirecki-Millunchick, and P. Bhattacharya, "High performance red-emitting multiple layer ingan/gan quantum dot lasers," Jpn. J. Appl. Phys. **55**(3), 032101 (2016).
11. K. Li, X. Liu, Q. Wang, S. Zhao, and Z. Mi, "Ultralow-threshold electrically injected algan nanowire ultraviolet lasers on si operating at low temperature," Nat. Nanotechnol. **10**(2), 140–144 (2015).
12. D. J. Paul, A. A. Mimi, A. Hazari, P. Bhattacharya, and M. Z. Baten, "Finite-difference time-domain analysis of the tunability of Anderson localization of light in self-organized GaN nanowire arrays," J. Appl. Phys. **125**(4), 043104 (2019).

13. M. I. Tahmid, D. J. Paul, and M. Z. Baten, "Emergence and tunability of transmission gap in the strongly disordered regime of a dielectric random scattering medium," Opt. Express **29**(11), 17215–17226 (2021).
14. M. Rashidi, Z. Li, C. Jagadish, S. Mokkapati, and H. H. Tan, "Controlling the lasing modes in random lasers operating in the anderson localization regime," Opt. Express **29**(21), 33548–33557 (2021).
15. W. Ma, Z. Liu, Z. A. Kudyshev, A. Boltasseva, W. Cai, and Y. Liu, "Deep learning for the design of photonic structures," Nat. Photonics **15**(2), 77–90 (2021).
16. S. So, T. Badloe, J. Noh, J. Rho, and J. Bravo-Abad, "Deep learning enabled inverse design in nanophotonics," Nanophotonics **9**(5), 1041–1057 (2020).
17. J. Jiang, M. Chen, and J. A. Fan, "Deep neural networks for the evaluation and design of photonic devices," Nat. Rev. Mater. **6**(8), 679–700 (2021).
18. Z. Liu, D. Zhu, S. P. Rodrigues, K.-T. Lee, and W. Cai, "Generative Model for the Inverse Design of Metasurfaces," Nano Lett. **18**(10), 6570–6576 (2018).
19. I. Malkiel, M. Mrejen, L. Wolf, and H. Suchowski, "Inverse design of unparametrized nanostructures by generating images from spectra," Opt. Lett. **46**(9), 2087–2090 (2021).
20. I. Malkiel, M. Mrejen, A. Nagler, U. Arieli, L. Wolf, and H. Suchowski, "Plasmonic nanostructure design and characterization via Deep Learning," Light: Sci. Appl. **7**(1), 60 (2018).
21. C. C. Nadell, B. Huang, J. M. Malof, and W. J. Padilla, "Deep learning for accelerated all-dielectric metasurface design," Opt. Express **27**(20), 27523 (2019).
22. P. R. Wiecha and O. L. Muskens, "Deep Learning Meets Nanophotonics: A Generalized Accurate Predictor for near Fields and Far Fields of Arbitrary 3D Nanostructures," Nano Lett. **20**(1), 329–338 (2020).
23. R. Li, X. Gu, K. Li, Y. Huang, Z. Li, and Z. Zhang, "Deep learning-based modeling of photonic crystal nanocavities," Opt. Mater. Express **11**(7), 2122 (2021).
24. T. Asano and S. Noda, "Iterative optimization of photonic crystal nanocavity designs by using deep neural networks," Nanophotonics **8**(12), 2243–2256 (2019).
25. T. Asano and S. Noda, "Optimization of photonic crystal nanocavities based on deep learning," Opt. Express **26**(25), 32704 (2018).
26. W. Ma, F. Cheng, Y. Xu, Q. Wen, and Y. Liu, "Probabilistic Representation and Inverse Design of Metamaterials Based on a Deep Generative Model with Semi-Supervised Learning Strategy," Adv. Mater. **31**(35), 1901111 (2019).
27. Z. Liu, D. Zhu, S. P. Rodrigues, K.-T. Lee, W. Cai, J. Jiang, D. Sell, S. Hoyer, J. Hickey, J. Yang, and J. A. Fan, "Free-Form Diffractive Metagrating Design Based on Generative Adversarial Networks," ACS Nano **18**(8), 8872–8878 (2019).
28. E. Ashalley, K. Acheampong, L. V. Besteiro, P. Yu, A. Neogi, A. O. Govorov, and Z. M. Wang, "Multitask deep-learning-based design of chiral plasmonic metamaterials," Photonics Res. **8**(7), 1213 (2020).
29. N. B. Roberts and M. Keshavarz Hedayati, "A deep learning approach to the forward prediction and inverse design of plasmonic metasurface structural color," Appl. Phys. Lett. **119**(6), 061101 (2021).
30. J. Baxter, A. Calà Lesina, J. M. Guay, A. Weck, P. Berini, and L. Ramunno, "Plasmonic colours predicted by deep learning," Sci. Rep. **9**(1), 8074 (2019).
31. J. He, C. He, C. Zheng, Q. Wang, and J. Ye, "Plasmonic nanoparticle simulations and inverse design using machine learning," Nanoscale **11**(37), 17444–17459 (2019).
32. T. Zhang, J. Wang, Q. Liu, J. Zhou, J. Dai, X. Han, Y. Zhou, and K. Xu, "Efficient spectrum prediction and inverse design for plasmonic waveguide systems based on artificial neural networks," Photonics Res. **7**(3), 368–380 (2019).
33. T. Christensen, C. Loh, S. Picek, D. Jakobović, L. Jing, S. Fisher, V. Ceperic, J. D. Joannopoulos, and M. Soljačić, "Predictive and generative machine learning models for photonic crystals," Nanophotonics **9**(13), 4183–4192 (2020).
34. S. Chugh, A. Gulistan, S. Ghosh, and B. M. A. Rahman, "Machine learning approach for computing optical properties of a photonic crystal fiber," Opt. Express **27**(25), 36414 (2019).
35. S. Yu, X. Piao, and N. Park, "Machine learning identifies scale-free properties in disordered materials," Nat. Commun. **11**(1), 4842 (2020).
36. N. Borhani, E. Kakkava, C. Moser, and D. Psaltis, "Learning to see through multimode fibers," Optica **5**(8), 960 (2018).
37. Y. Li, Y. Xue, and L. Tian, "Deep speckle correlation: a deep learning approach toward scalable imaging through scattering media," Optica **5**(10), 1181 (2018).
38. A. Hazari, A. Aiello, T.-K. Ng, B. S. Ooi, and P. Bhattacharya, "Iii-nitride disk-in-nanowire 1.2 μm monolithic diode laser on (001) silicon," Appl. Phys. Lett. **107**(19), 191107 (2015).
39. M. Sakai, Y. Inose, K. Ema, T. Ohtsuki, H. Sekiguchi, A. Kikuchi, and K. Kishino, "Random laser action in gan nanocolumns," Appl. Phys. Lett. **97**(15), 151109 (2010).
40. A. N. Haque, T. Ahmed, and M. Z. Baten, "In-plane directionality control of strongly localized resonant modes of light in disordered arrays of dielectric scatterers," Opt. Express **29**(24), 39227–39240 (2021).
41. D. J. Paul, S. Hossain, and M. Z. Baten, "Disorder induced rotational-symmetry breaking to control directionality of whispering gallery modes in circularly symmetric nanowire assembly," Opt. Express **27**(16), 23645–23653 (2019).
42. A. F. Oskooi, D. Roundy, M. Ibanescu, P. Bermel, J. D. Joannopoulos, and S. G. Johnson, "Meep: A flexible free-software package for electromagnetic simulations by the fdtd method," Comput. Phys. Commun. **181**(3), 687–702 (2010).

Optics EXPRESS

43. V. A. Mandelshtam and H. S. Taylor, "Harmonic inversion of time signals and its applications," J. Chem. Phys. **107**(17), 6756–6769 (1997).
44. A. Mountassir, H. Benbrahim, and I. Berrada, "An empirical study to address the problem of unbalanced data sets in sentiment classification," in *2012 IEEE international conference on systems, man, and cybernetics (SMC)*, (IEEE, 2012), pp. 3298–3303.
45. M. Chen, X. Shi, Y. Zhang, D. Wu, and M. Guizani, "Deep Feature Learning for Medical Image Analysis with Convolutional Autoencoder Neural Network," IEEE Trans. Big Data **7**(4), 750–758 (2021).
46. N. Rashid, M. A. F. Hossain, M. Ali, M. I. Sukanya, T. Mahmud, and S. A. Fattah, "Autocovnet: Unsupervised feature learning using autoencoder and feature merging for detection of covid-19 from chest x-ray images," Biocybern. Biomed. Eng. **41**(4), 1685–1701 (2021).
47. A. Ng, "Sparse autoencoder," CS294A Lecture notes **72**, 1–19 (2011).
48. Z. Mnasri, S. Rovetta, and F. Masulli, "Audio surveillance of roads using deep learning and autoencoder-based sample weight initialization," *20th IEEE Mediterranean Electrotechnical Conference, MELECON 2020 - Proceedings* pp. 99–103 (2020).
49. M. F. Ferreira, R. Camacho, and L. F. Teixeira, "Using autoencoders as a weight initialization method on deep neural networks for disease detection," BMC Med. Inf. Decis. Making **20**(S5), 141 (2020).
50. J. H. Jang, T. Y. Kim, H. S. Lim, and D. Yoon, "Unsupervised feature learning for electrocardiogram data using the convolutional variational autoencoder," PLoS One **16**(12), e0260612 (2021).
51. D. P. Kingma and J. Ba, "Adam: A method for stochastic optimization," arXiv, preprint arXiv:1412.6980 (2014).
52. Y. Li, Y. Wang, S. Qi, Q. Ren, L. Kang, S. D. Campbell, P. L. Werner, and D. H. Werner, "Predicting scattering from complex nano-structures via deep learning," IEEE Access **8**, 139983–139993 (2020).
53. X. Ma, Y. Ma, P. Cunha, Q. Liu, K. Kudtarkar, D. Xu, J. Wang, M. Liu, M. C. Hipwell, and S. Lan, "A universal deep learning strategy for designing high-quality-factor photonic resonances," arXiv, preprint arXiv:2105.03001 (2021).
54. A. Mafi, "Transverse anderson localization of light: a tutorial," Adv. Opt. Photonics **7**(3), 459–515 (2015).
55. Q. Song, L. Liu, and L. Xu, "Directional random-laser emission from bragg gratings with irregular perturbation," Opt. Lett. **34**(3), 344–346 (2009).
56. S. Skipetrov, "Localization of light in a three-dimensional disordered crystal of atoms," Phys. Rev. B **102**(13), 134206 (2020).
57. J. Haberko, L. S. Froufe-Pérez, and F. Scheffold, "Transition from light diffusion to localization in three-dimensional amorphous dielectric networks near the band edge," Nat. Commun. **11**(1), 4867 (2020).